



# Characterization and tribological evaluation of NiCrMoNb and NiCrBSiC laser cladding on near- $\alpha$ titanium alloy

N. Jeyaprakash<sup>1,2</sup> · Che-Hua Yang<sup>1,2</sup> · Sheng-Po Tseng<sup>1,2</sup>

Received: 14 August 2019 / Accepted: 25 November 2019 / Published online: 19 December 2019  
© Springer-Verlag London Ltd., part of Springer Nature 2019

## Abstract

In the present study, two different types of coatings such as NiCrMoNb and NiCrBSiC were produced on titanium alloy using a high power Yb:YAG disk laser. Then the coatings were analysed to expose their phase characterization, microstructure and hardness using X-ray diffraction analysis (XRD), energy-dispersive spectroscopy (EDS), scanning electron microscopy (SEM), optical microscopy (OM) and Vickers microhardness machine (HV). Further, tribotest was performed through ball-on-plate machine to analyse the wear properties of coatings. In addition, worn surfaces of cladding and surface roughness were examined using FE-SEM and whitelight interferometer, respectively. The results showed that the both NiCrMoNb and NiCrBSiC cladding exhibited a dendrite homogeneous structure due to higher cooling rates. XRD results indicating that the solid solution of  $\gamma$ -Ni was mixed with chromium, boride, silicon and formed the structure of interdendritic eutectics on cladding region. Microhardness of the clad layer has remarkably been increased than substrate. The results of friction coefficient of specimen with NiCrBSiC are lower than that of specimens NiCrMoNb clad and substrate. Also, the wear resistance of NiCrBSiC clad has been increased than NiCrMoNb clad and substrate sample, which reveals that NiCrBSiC laser cladding plays a major role on wear resistance. The microstructures of NiCrMoNb and NiCrBSiC cladding layer are composed of Ni-rich austenitic, Cr, Mo, Nb and carbide, borides, respectively. The analysed wear track indicates that adhesion and abrasion was a major wear mechanism. The NiCrSiBC cladged worn-out surfaces exhibited reduction in surface roughness than NiCrMoNb clad and substrate.

**Keywords** Titanium alloy · NiCrMoNb · NiCrBSiC · Cladding · Microstructure · Wear mechanism · Surface roughness

## Highlights

- Two different types of coatings such as NiCrMoNb and NiCrBSiC were produced on titanium alloy. Both claddings were free from defects and achieved good metallurgical bonding.
- In NiCrSiBC coating, the elements such as carbon, boron and chromium were segregated as carboborides and carbides.
- The material loss on substrate is more than both cladding surfaces and abrasive; adhesive is identified as a major wear mechanism
- Comparing with NiCrMoNb and unclad specimen, the NiCrSiBC-cladged worn-out surfaces exhibited reduction in roughness average. Finally, the NiCrSiBC cladding can be considered an alternative to the NiCrMoNb coating.

✉ N. Jeyaprakash  
prakash84gct@gmail.com; prakash@ntut.edu.tw

Che-Hua Yang  
chyang@ntut.edu.tw

Sheng-Po Tseng  
tseng3392@gmail.com

<sup>1</sup> Centre of Mass Customization Additive Manufacture, National Taipei University of Technology, Taiwan, Republic of China

<sup>2</sup> Institute of Manufacturing Technology, National Taipei University of Technology, Taiwan, Republic of China

## 1 Introduction

Titanium-based alloys are widely used in marine, aerospace, automobile, biomedical, power generation and chemical industries due to their remarkable properties such as low weight, excellent corrosion, high specific strength, good biocompatibility and oxidation resistance [1]. But, due to poor tribological properties, the application of titanium alloys was restricted severally [2, 3]. Material loss from the specimen due to unconditional friction and higher impact on the mating surfaces is fundamentally a surface-associated phenomenon. The wear rate is mainly based on material structure and composition of the surfaces concerned. Hence, the wear resistance may be improved through suitable surface modification technique. Application of surface protection through pack cementation, diffusion bonding etc. has been the conventional practices for ages. Also, they are not environmentally supporting, time consuming and require complex heat treatment process. The concentrated energy beams such as electron, ion and laser-aided surface modification provide superior surface properties than conventional process. However, electron and ion beam processing is perfect for deeper penetration and shallow depth surface modification, respectively.

In terms of the flexibility, process economy and ease of operation, laser-based surface modification is more suitable for altering the surface of metallic substrates. Laser-based surface modification had great significance in changing the surface regions of reactive metals like titanium-based alloys. Laser surface modification includes laser alloying [4], laser remelting [5, 6], laser cladding [7] etc. Among these techniques, the coating produced by laser cladding shows good metallurgical bonding with the substrate and exhibits dense microstructure [8]. Xu et al. [9] investigated TiC-reinforced Inconel-625 laser cladding on stainless steel. The results showed that the refined microstructure was obtained and significantly improved the coating properties. Zhuang et al. [10] prepared Ni–Ti–Si laser cladding on Ti-64 substrate. The results indicated that the produced laser cladding increased wear resistance and microhardness. Yin et al. [11] examined the wear behaviour of titanium alloy by laser shock peening. The achieved results showed that wear resistance had improved due to enhancement in hardness.

On another hand, hardfacing of alloy powders has been a practice for a long time to enhance the tribological properties of metals. In recent years, Ni-, Fe- and Cobased hardfacing powders are used in many applications due to its excellent wear properties, high hardness and thermal resistance. Among these powders, nickel-based Inconel-625 and Colmonoy-5 had attracted more attention as a wear resistance coating. Hemmati et al. [12] studied the dilution effects of Ni–Cr–B–Si–C alloys on steel substrate and concluded that higher Fe fractions can form with Cr borides by increasing

the Fe content up to 25 wt.%. The primary chromium carbide completely suppressed the precipitation by further increasing Fe up to 40 wt.%. Ramasubbu et al. [13] investigated the effect of dilution of Colmonoy-6 (NiCr-C) on 316 SS metal using gas tungsten arc welding (GTAW). The results indicated that boride fraction was increased from 5 to 8% with a reduction in dilution. The formation of borides suppresses the high dilution base material and is responsible for the lower hardness on the deposit. Fernandes et al. [14] examined the oxidation behaviour of nickel-based hardface coating on grey cast iron using plasma-transferred arc (PTA) method. Kumar et al. [15] studied the wear behaviour of tungsten inert gas (TIG)-deposited Ni–Cr–B coating on 316LN SS. The final outcome shows that improved wear resistance and friction coefficient were observed on Ni–Cr–B coatings. Paolo Sassatelli et al. [16] examined the properties of Stellite-6 coating using high-velocity oxy-fuel (HVOF) coating. The results indicated that microstructure has a major role on corrosion resistance of the coating. Further, the wear behaviour has less influence on the microstructure. Ferozhkhan et al. [17] studied the wear resistance of Stellite-6 coating using PTA. The final outcomes showed that the wear resistance was improved through PTA hardfacing and is useful in valve application in high temperature.

From the above literature, it is clear that GTAW, PTA, TIG and HVOF technology were used to coat the powders on substrate material. Major research works focused on HVOF-sprayed Stellite coatings on corrosion resistance [18]. On the other hand, Stellite and Colmonoy laser cladding were investigated by few researchers by considering their coating structure [19], processing parameters [20] and dilution effects [12, 13]. However, no literature was found on tribological comparison of NiCrMoNb and NiCrBSiC laser cladding on titanium material using high-power Yb:YAG disk laser. As laser material processing becomes more extensive in the industry, the research and development of their application in the field of surface modification change their attention from standard applications such as laser hardening or melting to advanced techniques, e.g. laser cladding or alloying. The comparison of two various hardfacing depositions by laser cladding provides better understanding in enhancing the properties of the surfaces.

In the present study, phase analysis, microstructure and hardness of NiCrMoNb and NiCrBSiC depositions were examined using X-ray diffraction analysis (XRD), field emission scanning electron microscopy (FE-SEM), energy-dispersive spectroscopy (EDS) and Vickers microhardness tester. Further, wear resistance of the deposited coatings was investigated using ball-on-plate tribometer. In addition, wear mechanism of worn-out surfaces and roughness averages (Ra) was analysed and reported using FE-SEM and whitelight interferometer, respectively.

## 2 Experimental

### 2.1 Materials

In this study, titanium alloy was used as a substrate material with a dimension of  $50 \times 50 \times 10$  mm. The surface of the material was polished with silicon carbide grit papers to obtain a surface roughness of  $\sim 7$   $\mu\text{m}$ . Commercially available nickel-based NiCrMoNb (Inconel-625) and NiCrBSiC (Colmonoy-5) powders were used as coating materials. SEM picture of the powders is shown in Fig. 1, and the powder was in spherical shape with a particle size of 30–125  $\mu\text{m}$ . The chemical composition of the powders and substrate is shown in Table 1.

### 2.2 Laser cladding

A high-power Yb:YAG disk laser was used to clad the selected powders on substrate material. The wavelength of laser beam was about 1030 nm and circular shape beam mode was applied. A deposition at 300- $\mu\text{m}$ -thick NiCrMoNb and NiCrBSiC alloy powders was separately exposed to the laser source. The process parameters such as power (W), scanning speed (mm/min) and feed rate (g/min) varied, and optimized laser clad parameter based on defect free and good bonding of the coating was found.

The Gaussian-based laser beam is not suitable to perform laser cladding works (deep bulk material damage, high dilution); specifically today, various beam-shaping methods and high-power laser sources are investigated for applications which require uniform distribution and larger spot. The use of a disk-type laser permits to produce uniform distribution with a large-spot diameter [21]. The produced laser source focused on the titanium surface, and a melt pool was formed. The selected powders were blown simultaneously into the laser source and formed a melt pool [22]. Argon (25 l/min) was used as a shielding gas to evade unwanted oxidation process in the clad region. The tip of the nozzle was kept 15 mm away from the specimen surface. The angle used between specimen and nozzle was exactly perpendicular. The parameters used for the laser cladding are shown in Table 2. The hard powders absorbed some laser heat and incompletely melted before reaching the substrate surface. Also, substrate material received a part of the laser energy for its melting. The value of laser beam fluence ( $F$ ) can be measured using Eq. (1).

$$F = \frac{PE_t}{\pi r^2} \quad (1)$$

where  $P$  is the power of laser beam in watts,  $E_t$  represents the exposure time in seconds and  $r$  indicates the laser beam radius in millimetres. The laser  $E_t$  on material can be calculated according to the Eq. (2).

**Fig. 1** SEM picture of as-received alloy powders **a, b** NiCrMoNb and **c, d** NiCrBSiC

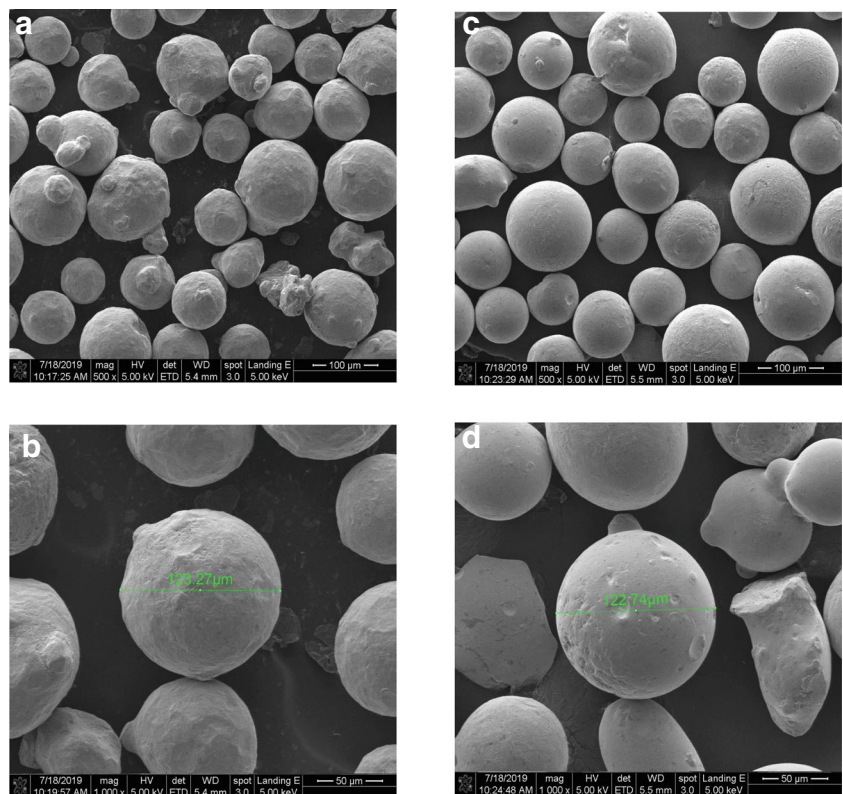


**Table 1** Chemical composition of powders and substrate

Materials	Elements compositions (wt.%)											
	Fe	Ni	C	Ti	Al	Zr	Mo	Cr	Mn	Si	Nb	B
NiCrMoNb	0.67	Bal	0.10	–	–	–	8.9	21.3	0.39	0.42	3.58	–
NiCrBSiC	4.4	Bal	0.6	–	–	–	–	11.5	0.1	3.8	–	2.6
Substrate	–	–	–	Bal	6.0	5.0	0.5	–	–	0.25	–	–

$$E_t = \frac{d}{v} \quad (2)$$

where  $d$  represents diameter of laser beam in millimetres and  $v$  denotes the scanning velocity of laser beam in millimetres per minute. NiCrMoNb and NiCrBSiC clad were formed in six passes and after completing every pass, the laser heads back to the original position and is lifted by 1 mm. The schematic picture of laser cladding process and samples after cladding is shown in Fig. 2.

### 2.3 Specimen preparation and characterization

The suitable samples for experimental work were cut from the coated blocks through resin-bonded alumina blades by applying constant lubricants. For microhardness and FE-SEM examination, the clad samples were cross-sectioned at room temperature. Also, the coated specimen was cut into plate shape with dimensions of  $40 \times 40 \times 10$  mm for the wear test. Then, the sectioned samples were roughly polished with different grit size papers and alumina paste was used to achieve mirror polishing to reveal the microstructure. The chemicals such as 2 g copper chloride, 40 mL HCL and 50 mL ethanol were used to etch the samples.

The powder particle size and coating cross-section were examined using optical microscopy (OM) (Olympus) and FE-SEM (JEOL-JSM-7610F) equipped with EDS. The produced coating thickness (300  $\mu\text{m}$ ) were measured and confirmed with optical microscopy. The coating cross-sections are shown in Fig. 3. X-ray diffraction study was conducted on both powders and clad

**Table 2** Laser cladding parameters

Power	1000 W
Scanning speed	600 mm/min
Feed rate	7 g/min
Spot size	3.2 mm
Stand-off	15 mm
Overlapping	50%
Powder carrier gas (argon)	6 SD at 1 bar
Shielding gas (argon)	25 lpm
Pre-heating	150 °C

surfaces using Cu-K $\alpha$  energy produced at 40 kV and 40 Ma. The observed patterns were analysed using X-pert high-score software to detect elemental compositions. Wolpert Wilson micro-indentation examination was performed to measure the hardness by applying the load of 300 g and 15 s dwell time. At least ten indentations were taken to measure the hardness on both clad regions. Further, wear mechanism of worn-out surfaces and surface roughness was analysed using FE-SEM and whitelight interferometer, respectively.

### 2.4 Wear study

Dry-sliding ball-on-plate wear study was conducted on both cladding surfaces as per ASTM G99-05 standard [23]. Figure 4 shows a schematic picture of ball-on-plate apparatus. The hardened tungsten carbide ball was used as a counterpart with the diameter of 6.22 mm diameter. Sliding velocity, applied load and sliding distance were selected as the wear study parameters. The plate weight was measured before and after the wear study to measure the mass loss. An electronic weighing machine was used to measure the mass loss with an accuracy of 0.1 mg. The volume loss and friction coefficient can be measured through the following Eqs. (3)–(6).

$$V = \frac{\text{Mass loss}}{\rho} \times 1000 \quad (3)$$

where  $V$  represents volume loss ( $\text{mm}^3$ ) and  $\rho$  indicates the density

$$\text{Sliding distance (m)} = \pi NDT \quad (4)$$

where  $N$  denotes rotational speed (rpm),  $D$  represents wear track diameter (m) and  $T$  indicates the time (min)

$$\text{Wear rate}(\text{mm}^3/\text{min}) = \frac{V}{d} \quad (5)$$

$$\text{Friction coefficient} (\mu) = \frac{F}{N} \quad (6)$$

where  $d$  represents sliding distance in metres,  $F$  indicates frictional force (N) and  $N$  means normal load (N).



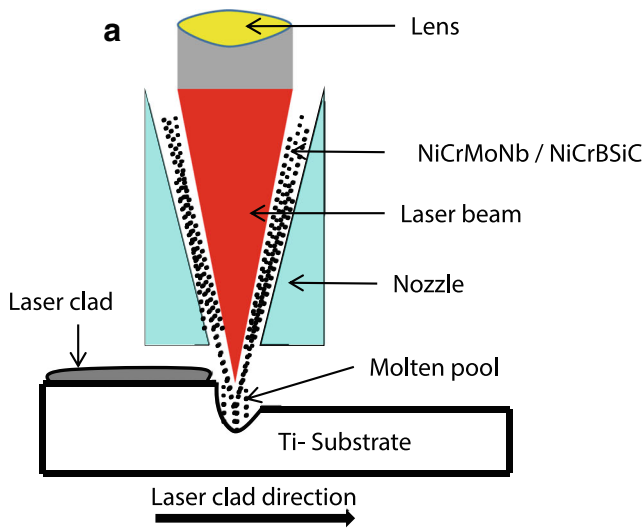


**Fig. 2** **a** Schematic of laser cladding process and **b** samples after laser cladding

### 3 Results and discussion

#### 3.1 Phase analysis

In order to identify the formed phase structure on the clad surface, X-ray analysis was conducted on top of the surfaces. X-ray analysis of NiCrMoNb cladding surface is shown in Fig. 5a. All the four peaks noticed with the corresponding

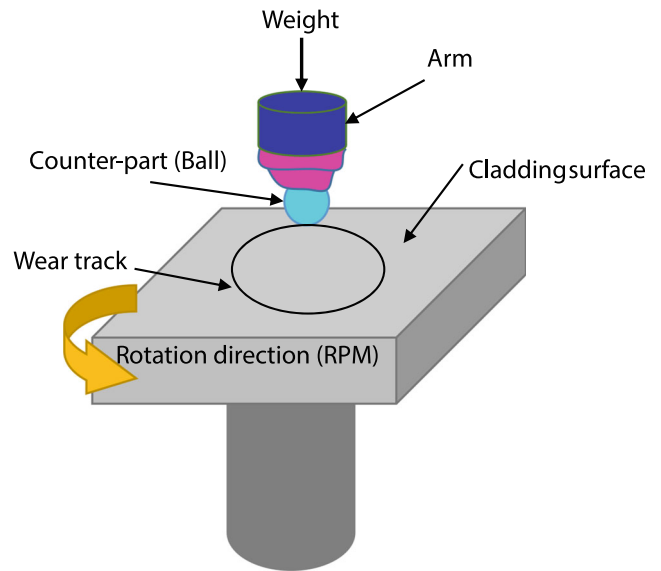


**Fig. 4** Schematic of ball-on-plate setup

diffracting planes, namely 111, 200, 220 and 311 are from the NiCrMoNb coating while the unmarked peaks are related to the substrate material [24]. Examination of peak positions and interplanar spacing ratios for the peaks corresponds to the NiCrMoNb coating a single-phase face-centred cubic (fcc) solid structure for the produced coating. The coating peaks showed a significant peak broadening and specified the presence of comparatively small crystallites in the coating microstructure while being compared with substrate peaks.

Based on the EDS results, the point A contains 17.4 wt.% Cr, 53.56 wt.% Ni, 5.2 wt.% Mo and 7.3 wt.% Nb. The phase  $\gamma$  usually have high percentage of solid soluble alloys like Mo and Cr with fcc structure. It can be concluded that point A has phase  $\gamma$ . There is a chance to form the  $\gamma$  phase in point B as it has nearly the same weight percentage as of point A. In point C, there is a probability for the formation of carbide phase by considering the weight percentage of carbon and chromium (42.3 wt.% Cr, 35.34 wt.% Ni, 8.1 wt.% Mo and 9.1 wt.% Nb). Based on the measured chemical composition of the intermetallic ( $Ni_3Nb$ ) compound, which is coherent with phase  $\gamma$ ,

**Fig. 3** Cross-sectional optical images of cladding: **a** NiCrMoNb and **b** NiCrBSiC

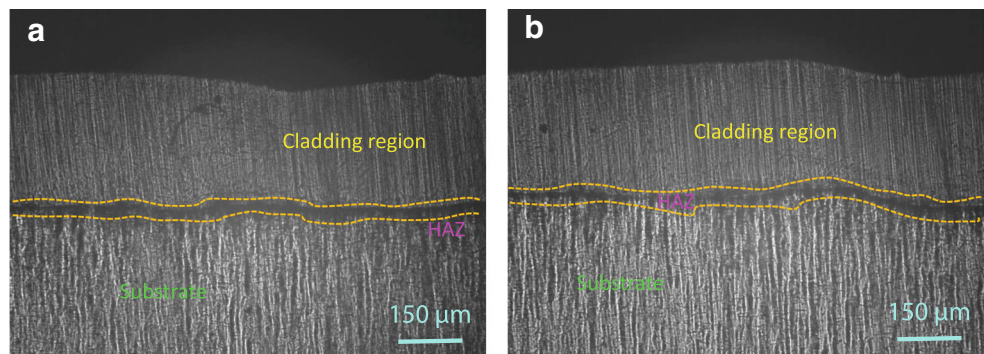
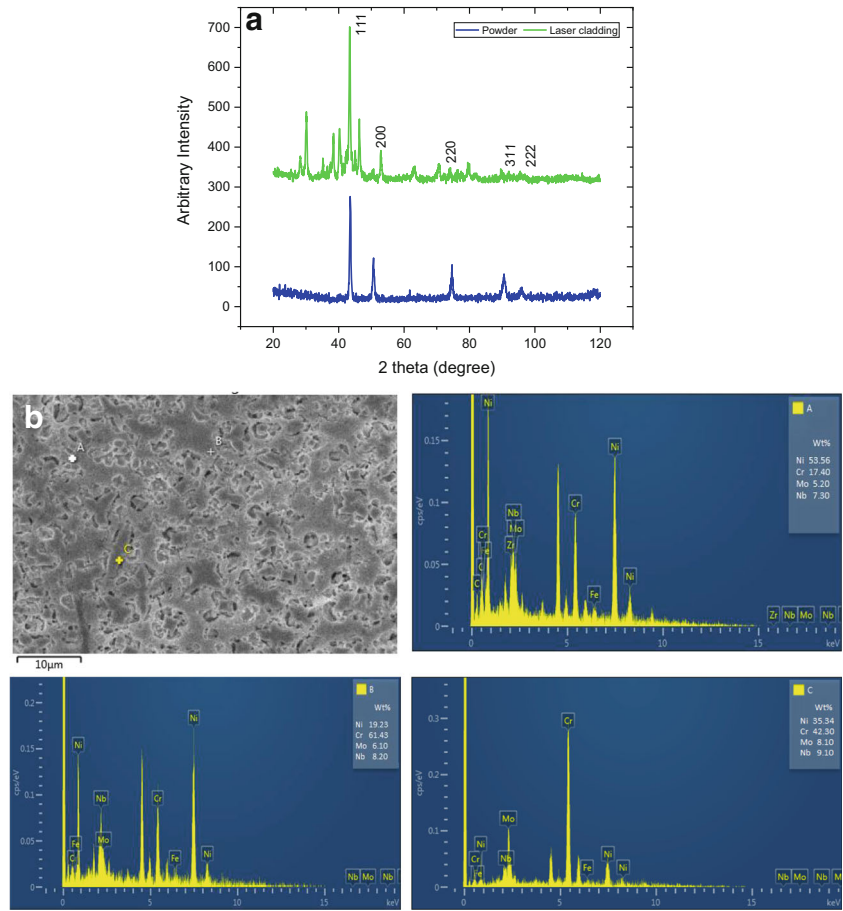
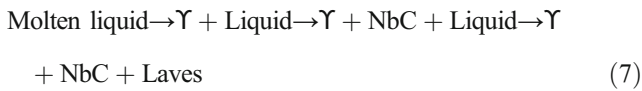


**Fig. 5** **a** XRD analysis of NiCrMoNb powders and cladding surface, **b** EDS analysis of three different points (points A–C) to study the elemental weight percentage distribution



the phase  $\Upsilon$  or  $Y$  can be formed. Then, there are chances to form a continuous Laves phase on the coaxial region due to less thermal gradient [25]. Normally, the solidification of NiCrMoNb begins with the formation of  $\Upsilon$  dendrite phase, whereby Mo and Nb elements can be deviated from the dendrite centre and reaches the molten dendrites. In another side, the elements such as iron, nickel and chromium can migrate to  $\Upsilon$  dendrites. The compounds such as Mo and Nb increases in the melt during the continuous solidification and then the compounds  $\gamma$ /Laves were obtained. Therefore, Laves +  $\Upsilon$  + NbC was formed. During the cladding process, crystallization trend of the NiCrMoNb is as follows Eq. (7) [26].



X-ray analysis of NiCrBSiC cladding surface is shown in Fig. 6. From the figure, it is confirmed that fcc  $\gamma$ -Ni was the most dominant peak among other peaks. The observed major peaks are related to nickel due to solid solution of matrix. Two major peaks such as  $\text{Cr}_5\text{B}_3$  and  $(\text{Ni, Fe})_3\text{B}$  were noticed from the X-ray analysis. In addition, carbides and borides ( $\text{CrB}$ ) were present on the laser cladding surface [27]. Mixing of  $\gamma$ -Ni and borides formed the structure of interdendritic eutectics. Therefore, the

SEM and XRD results strongly indicate that the black phase is chromium boride ( $\text{CrB}$ ). The reason for forming the chromium carbide phase was possibly due to the primary solidification process. Next, the grey phase was identified with the combination of iron-chromium carbide; this can be formed due to a local change of the primary solidification mode. In

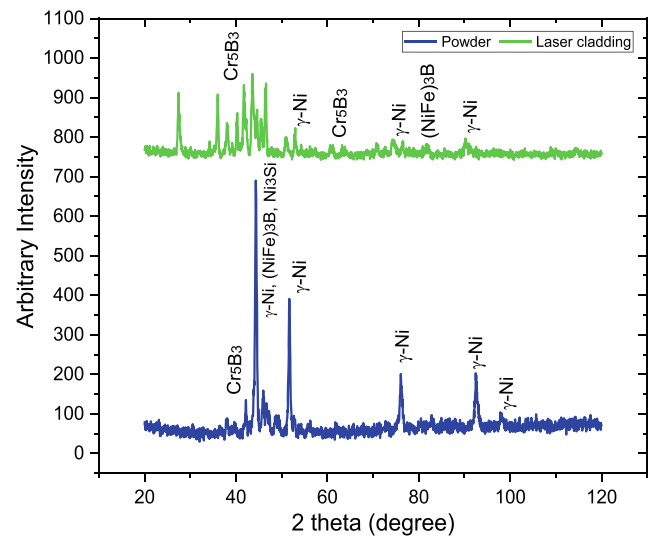


**Fig. 6** XRD analysis of NiCrMoNb powders and cladding surface

Colmonoy alloy series, the formation of borides and carbides over laser cladding was reported by Conde et al. [28]. Additionally, the period time of clad molten pool solidification, which is unavoidable in the creation of more eutectics, such as lamellar eutectics was noticed. The XRD analysis suggests that lamellar interdendritic eutectics are  $\gamma\text{Ni} + \text{Ni}_3\text{B}$  lamellar eutectic. Based on the observed microstructure, the darker interdendritic region is the solid solution of  $\gamma\text{-Ni}$  and the white dendritic area observed is the  $\text{Ni}_3\text{B}$  phase.

### 3.2 Microstructure analysis

Figure 7a–c shows the OM and FE-SEM pictures of NiCrMoNb cladding. The observed coating interface shows no defects such as porosity and cracks. The coating shows a finer and dendrite structure due to higher cooling rate. In the laser cladding process, the laser parameters were controlled properly and thus the heat source to the base metal and the melting of eutectic phases were controlled in grain boundary; therefore, the chances of crack development were controlled from the cladding region [29]. The top region of the coating showed a coaxial dendrite microstructure. The mid-region of the coating showed coaxial dendrites and a columnar structure, while the lower region shows columnar dendrites. The interface regions are showing cellular structure and the formation of dendrite structure due to constitutional undercooling. Undercooling needs a concentration gradient in the cooling front. At this situation, during the solidification process, the molten pool in the cooling front becomes rich in alloy elements.

The gradient temperature was reduced, and the rate of growth was enhanced from the molten pool towards the coating region [30]. Random orientation and non-uniformity were noticed on the cell and dendrite growth. In certain cases, those non-uniform orientations were randomized properly. The orientation of grow cells and dendrites specify that the temperature were mainly transferred by substrate material. Therefore, the direction of the heat flow during the cooling time is perpendicular to the substrate surface, which causes to form a directional dendritic [31]. This is due to the reason that there is a competition mode to developing the dendrite structure on the columnar region and has a tendency towards a direction, in which they develop effortlessly and, since the  $\Upsilon$  phase has the fcc structure, their effortless development in the way of (100) [32, 33]. Generally, laser cladding process shows a higher cooling rate in the molten pool region, and the cooling rate may be reduced in the direction of coating surface. Hence, there is no possibility to form the secondary arms on the lower molten pool region and final growth may be a cellular. Additionally, the measured heat-affected zone was less due to the selected laser cladding method which is the higher cooling rate.

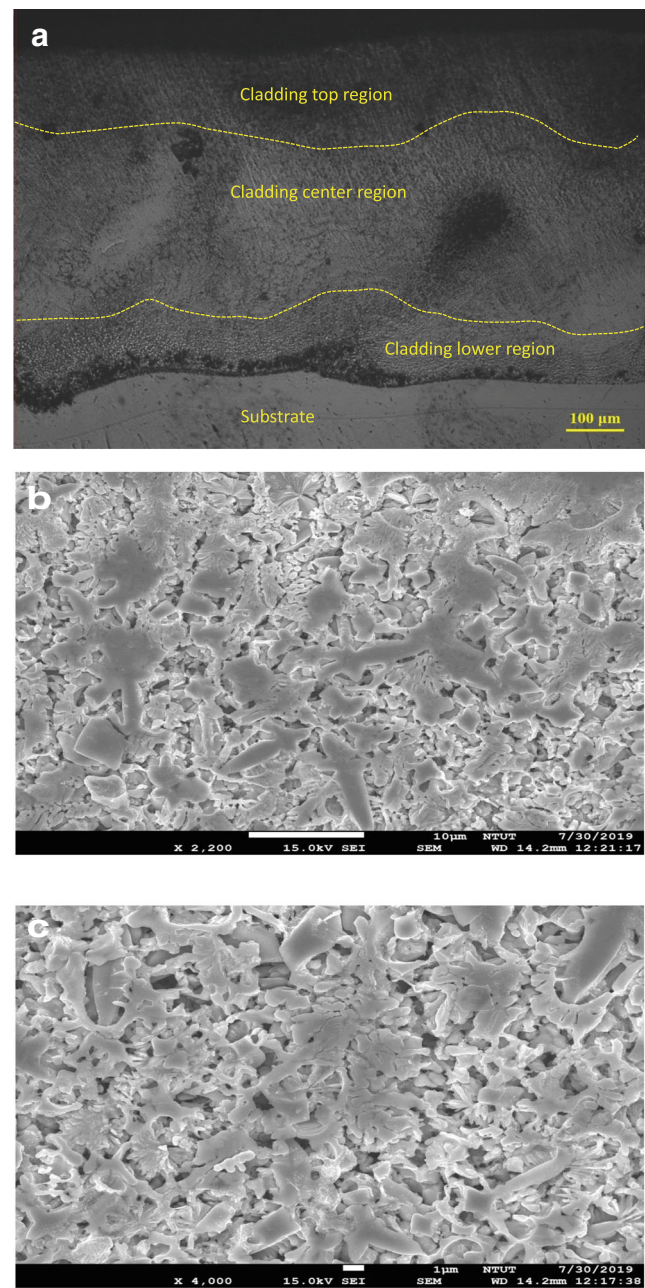


**Fig. 7** Cross-sectional OM picture shows the three different regions: cladding lower, centre, and top regions (a). FE-SEM picture of NiCrMoNb-cladded region with lesser (b) and higher magnifications (c)

Nickel-based NiCrBSiC alloy is a matrix of Colmonoy-5. The average content of Cr, B and C was 10–15% and dispersed in a solid matrix of Fe–Cr–Ni–B. The element distribution in NiCrBSiC is roughly as follows, chromium carboboride ( $\text{Cr}_{27}\text{BC}_4$ ) is 10 wt.%, chromium carbide ( $\text{Cr}_{23}\text{C}_6$ ) is 10 wt.%, chromium boride is 20 wt.% and chromium carbide ( $\text{Cr}_7\text{C}_3$ ) is 60 wt.%. The phases  $\text{Cr}_7\text{C}_3$  and  $\text{Cr}_{23}\text{C}_6$  have hexagonal close-packed structure and face-centred cubic structure, respectively. These phases are not pure ones as they contain the Ni–B–Fe matrix [34]. This



combination of matrix increases the hardness with the boron content, presently as chromium boride which is very brittle and hard. In NiCrBSiC coating, the elements such as carbon, boron and chromium were segregated as carboborides and carbides. Significant traces of iron and nickel were noticed in NiCrBSiC coatings. The coating shows dendrite structure due to the rapid cooling. In addition, the NiCrBSiC has less extended shape with small grain size than NiCrMoNb.

In NiCrBSiC coating, the structure shows a uniform dendrite growth towards the build-up direction. It included interdendrite constituent and primary dendrite structure. The EDS examination has revealed the dendrite to be  $\gamma$ -nickel and which also have other elements such as Si, Cr and Fe. The eutectic phases were observed to be between  $\gamma$ -nickel dendrites. The lighter areas observed between the phases are  $\gamma$ -nickel, while darker area of the eutectic remains boride [35]. The borides are showing largely as nickel borides. However, the EDS study shows that iron and chromium also were present. Therefore, eutectic interdendrite structures are nickel boride and binary eutectic of  $\gamma$ -nickel. The iron content decreases, the fusion line increases and finally eutectic structure was observed. The same observations were found by Zhang et al. [27] in their investigation of NiCrSiBC powders on SS316L through  $\text{CO}_2$  laser cladding. Figure 8a–d shows the OM, FE-SEM pictures and EDS analysis of NiCrBSiC cladding.

### 3.3 Microhardness

The microhardness was measured on the cross-section of laser clad samples. This investigation was made to evaluate the hardness variations on laser clad samples and substrate material. Figure 9a shows the schematic picture of microhardness indentation in different region, Fig. 9b shows cross-sectional SEM picture with coating thickness and Fig. 9c shows measured hardness profile across the cladding depth. The average microhardness of titanium alloy was  $335 \text{ HV}_{0.3}$ . After laser cladding with NiCrMoNb and NiCrSiBC alloy powders, the microhardness was enhanced by 1.75 times (avg.  $584 \text{ HV}_{0.3}$ ) and 2.72 times (avg.  $914 \text{ HV}_{0.3}$ ), respectively. The nickel-based NiCrMoNb and NiCrSiBC alloy powders was properly fused on the top surface of titanium alloy material as proved in the EDS analysis. The substrate dilution is unavoidable due to proper bonding with base metal. Hence, the small differences can be observed in the hardness profile due to substrate dilution. The difference in hardness profile within the coating could be due to temperature effect and subsequent microstructure modifications produced by laser cladding tracks [36]. This was verified practically that while a hard alloy powders were fused or/bonded on the softer surface, the hardness of the fused or bonded surface was improved [37]. Similarly, Pengting et al. [38] observed the same behaviour in fusion of hard alloy particle in smoother surface. It was due to the

dendrite structure restricting the plastic distortion created by the hardness indenter. Therefore, the dendrite/interdendrite structure has shown the greater strengthening effect on the laser clad region. Furthermore, the residual stress, which is produced by rapid heating and cooling through laser clad, might be reason to the enhancement of hardness. All the clad layers were achieved more hardness than substrate material due to the formation of solid nickel solutions.

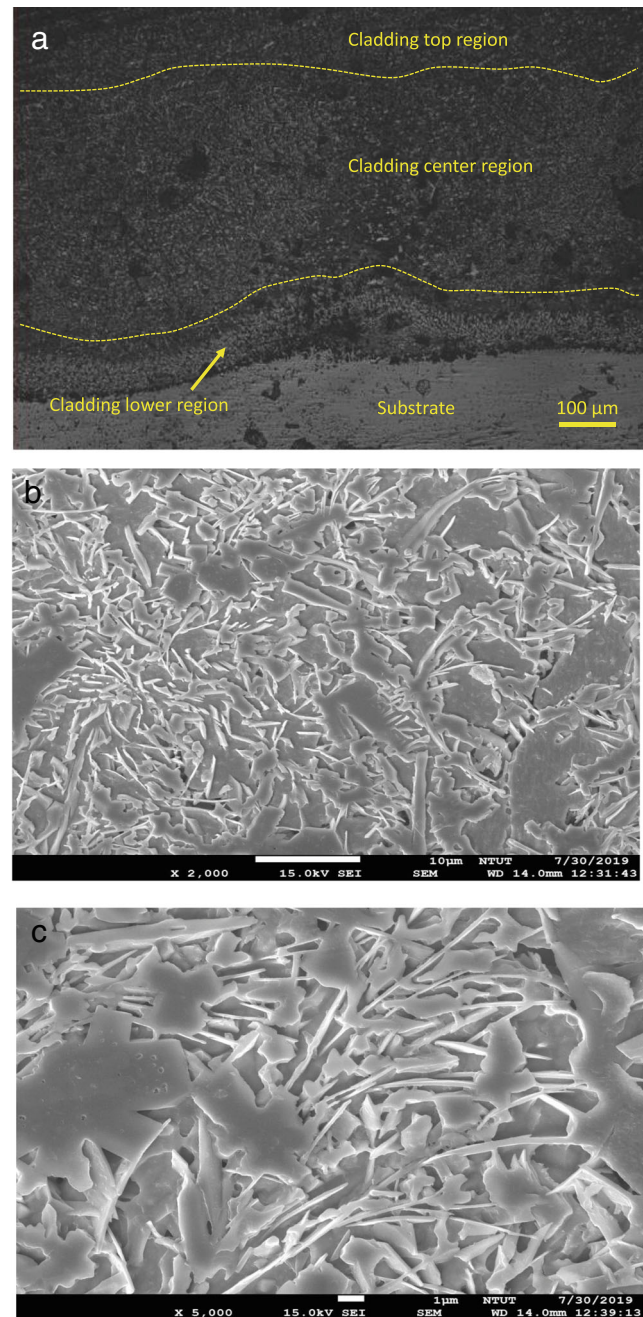


**Fig. 8** Cross-sectional OM picture shows the three different regions: cladding lower, centre, and top regions (a). FE-SEM picture of NiCrBSiC-cladded region with lesser (b) and higher magnifications (c). EDS analysis to study the elemental weight percentage distribution on two different points



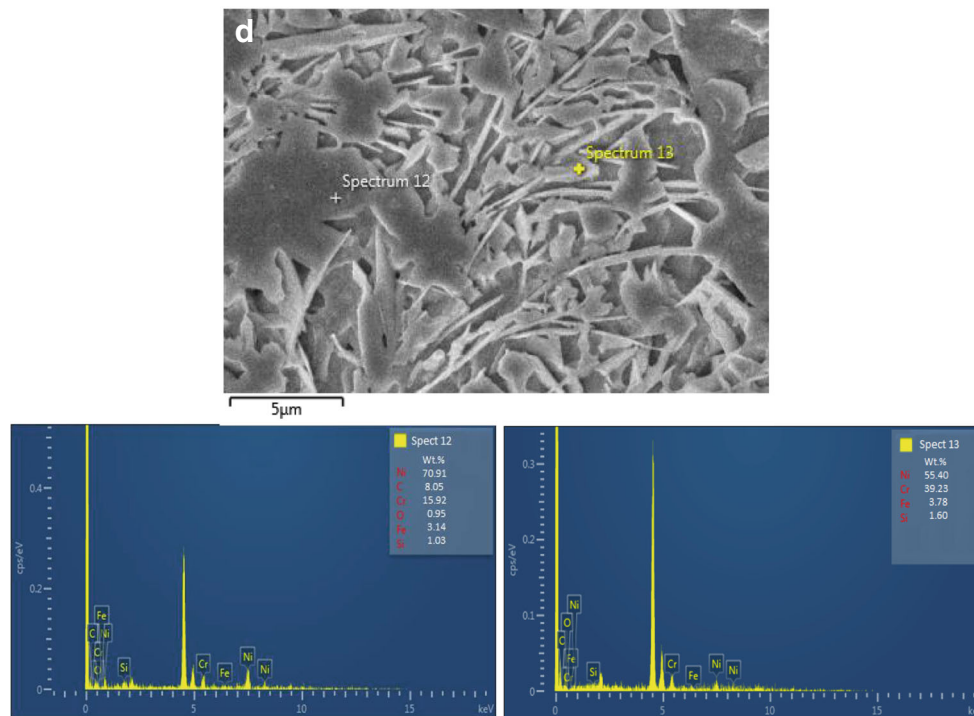


Fig. 8 (continued)

In the cladding zone, NiCrMoNb coating has hardness variations from 576.8 to 591.5 HV<sub>0.3</sub>. NiCrMoNb alloy, which is a solid solution, has improved the super alloy; the solid solution elements such as Nb and Mo were major elements in the hardness determination. So, as indicated in SEM and EDS results, finer structure and alleviated segregation of Nb and Mo helps hardness improvement in NiCrMoNb cladding. In NiCrSiBC cladding, boron (carbaborides) was identified in the harder particle components and is distributed evenly in the matrix. The element distribution and hardness is proving that the coating has a homogeneous structure. Moreover, the hardness measurement of NiCrSiBC appears higher than NiCrMoNb.

### 3.4 Wear and friction behaviour

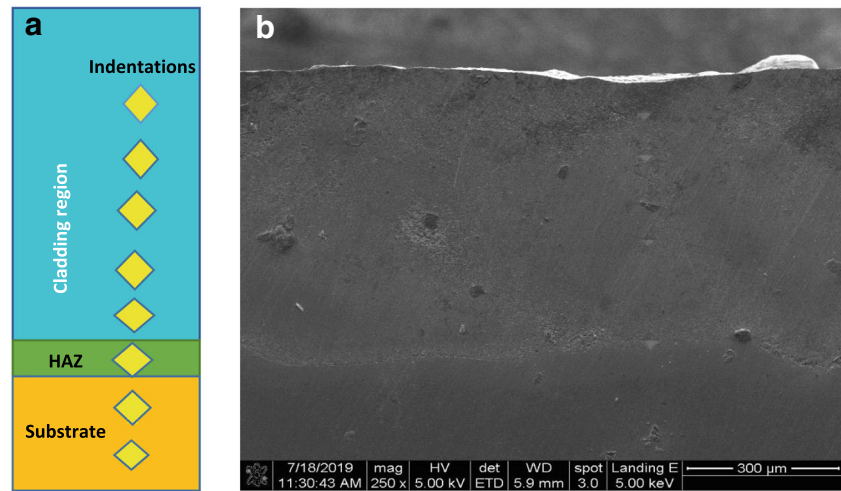
Wear resistance is one of the major properties arousing nearly all the tribologist attention, when the treated surfaces would be subject to friction. There are many of these cases with titanium alloys. Laser cladding is used widely to improve the tribological properties of titanium alloys. By choosing the proper parameters and materials, cladding exhibiting good wear resistance can be achieved.

Dry-sliding wear study results are presented in Fig. 10a, in which the total mass loss was compared with the sliding distance. Based on the achieved outcomes, it can be observed that the weight loss of the laser clad samples (NiCrMoNb and NiCrSiBC) is less than the substrate material. The material loss on the substrate was about ~2.25 g which is more than

~0.76 g (NiCrMoNb) and ~0.41 g (NiCrSiBC) for 2500 m sliding distance. This happened due to the enhancement of base-metal hardness after laser cladding with NiCrMoNb and NiCrSiBC powders. In the cladding period,  $\gamma$ -Ni was mixed with chromium, borides, silicon and molybdenum and formed the structure of interdendritic eutectics, which can provide a strong network to enhance the wear resistance of the cladding layer. Furthermore, the weight loss of the base metal increases while increasing the sliding distance. In the start condition, the laser clad samples increased the weight loss and after reaching some sliding distance, shows a stable condition due to the formation of the oxide layer through sliding surface [39]. The main reason to the formation of the oxide layer is the increase in the surface temperature. However, the oxide layers can be observed at lower temperatures. This predicted that rubbing between two surfaces increases the temperature at the contact surfaces. Therefore, the heat sources are locally increased and oxide layers were formed [40]. Those formed oxides get entrapped between two contact surfaces or they can be detached in the form of wear debris thus developing a layer to protect the NiCrMoNb/NiCrSiBC surfaces and improve the wear resistance.

The friction coefficient is one of the effective ways to analyse the wear performance of the clad/coated samples and lesser friction coefficient is often regarded as improved wear resistance. The substrate (titanium) material shows a high and unstable friction coefficient while sliding against WC ball. As shown in Fig. 10b, the friction trace of titanium alloy sliding against WC ball in air can fluctuate during the complete

**Fig. 9** **a** Schematic picture of microhardness indentation in three different regions: cladding region, heat-affected zone and substrate; **b** cross-sectional SEM picture showing three different regions; **c** microhardness profile of laser-cladded cross-section



testing period, representing the stick-slip adhesive wear while sliding against the WC ball. The physical interaction between testing surface and counter body surface increases when increasing tangential force over junction growth and both contact surfaces remain in adhesive, showing a ‘stick’. Then, while the applied force exceeds the adhesive strength, the junction ruptures and a rapid ‘slip’ for both surfaces can occur. This stick-slip series happened repeatedly, accounting for the friction force fluctuation.

From the plotted graph, it can be observed that the coefficient of friction of both NiCrMoNb and NiCrSiBC coatings are 0.65 and 0.55, respectively. In general, the trend of friction curve can be separated in two stages, wearing-in stage and stable wearing stage. In the wearing-in stage, both cladded NiCrMoNb and NiCrSiBC coatings are showing instable friction coefficient at the starting stage of the test. At the starting time of sliding between two pairs, the interfacial film will be abraded and mismatch contact points will be occurring

between two mating pairs. Therefore, a high shear force is required to remove the mismatch points and consequently the produced friction coefficient is a little higher than that stable wearing stage. On the other side, it can be observed that the stable wearing stage shows the constant friction coefficient around 0.57–0.60 (NiCrMoNb) and 0.47–0.50 (NiCrSiBC). This behaviour may be attributed due to various wear mechanisms during wear test.

In the beginning time of sliding, both NiCrMoNb and NiCrSiBC cladding surface undergo abrasive wear process, in which the surfaces wear off from contacting pairs act as abrasive, as a result higher coefficient of friction was produced [41]. Then, after sliding some distance, the friction pairs may produce some debris and can be easily transferred between two contacting surfaces. Hence, the adhesive wear is the most leading mechanism after crossing some sliding distance or temperatures. The wear tracks of NiCrMoNb and NiCrSiBC coatings are showing less wear debris on worn-out surface. In

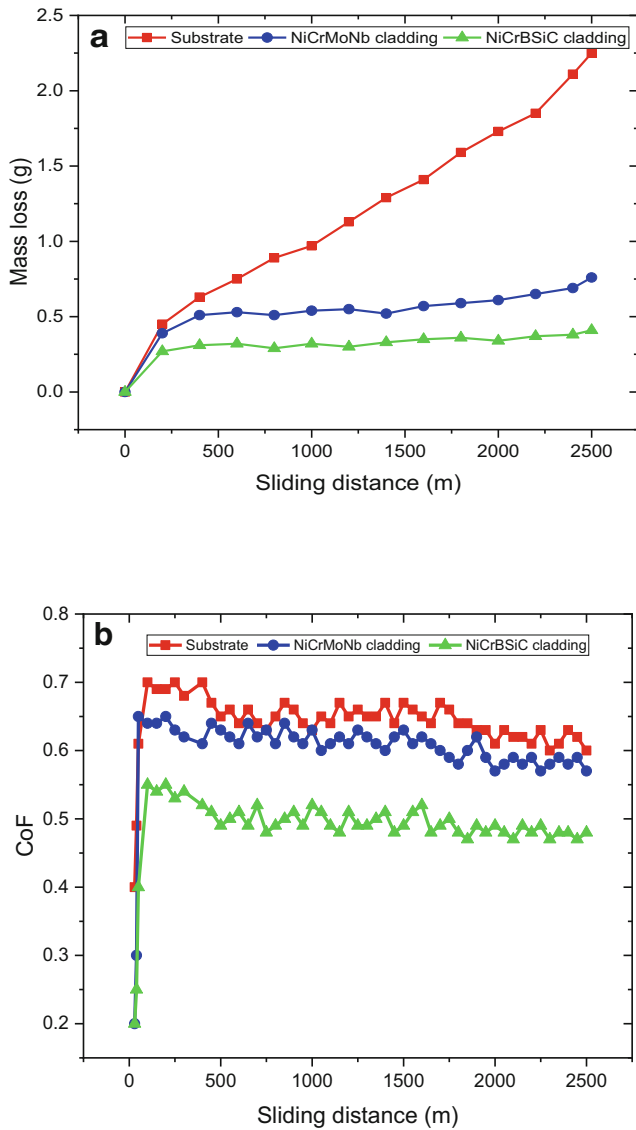


Fig. 10 a Mass loss; b CoF of substrate and laser-cladded samples

comparison, NiCrMoNb coating has deeper groove on wear tracks as compared with NiCrSiBC coating, indicating a higher wear rate.

The laser-cladded NiCrSiBC sample has lesser wear rate than the NiCrMoNb coating. In detail, the wear rate of NiCrMoNb shows highest (0.76 g), whereas that of the NiCrSiBC coating shows 0.41 g. The lower wear rate in NiCrSiBC was attributed due to carbon-boride matrix during this cladding process as confirmed by EDS results and corresponding higher hardness.

### 3.5 Wear mechanism

In general, titanium surface contacts with either ceramic or metallic, in motion or under force, adhesive wear can occur. The titanium alloy sliding against harder WC ball indicates the stick-slip behaviour [42]. This stick-slip process is closely

associated with strong adhesion of titanium. Figure 11a shows the FE-SEM picture of worn-out substrate sample. Based on the observation of substrate worn track, deeper grooves formed by ploughing as well as adhesive spots which are related to practically noted instability in the stick-slip friction process. From the substrate surface, it is noted that the material loss is high while comparing with laser-cladded specimens. The deeper finer grooves were visible on the untreated surfaces. This indicated that the plastic deformation is high in the untreated surface which confirms the less wear resistance to abrasion. However, the NiCrMoNb and NiCrSiBC laser-cladded samples had enhanced the wear resistance compared with the untreated specimen.

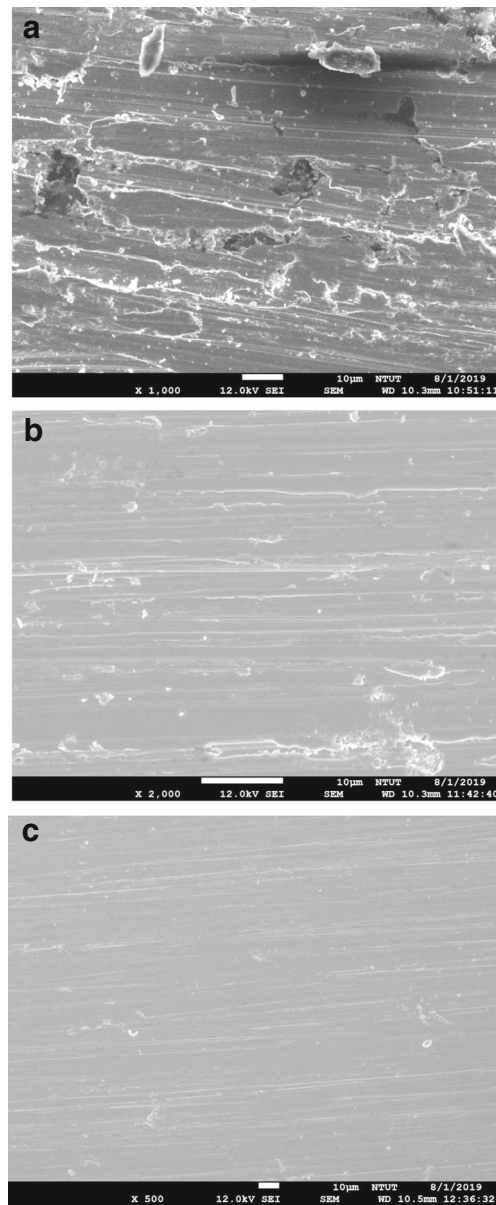


Fig. 11 SEM micrograph of worn-out cladded surfaces: a substrate, b NiCrMoNb and c NiCrSiBC

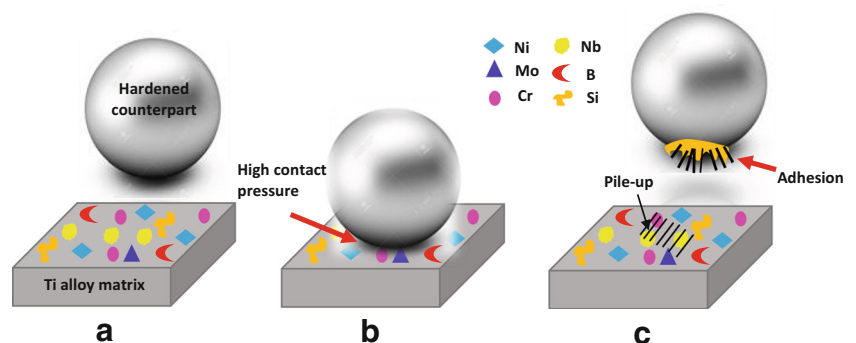


Figure 11b, c shows the wear track of laser-cladded samples. It can be observed that the wear track is mild on the cladded sample. In addition, the wear loss is less compared with the untreated specimen. When the cladded surface meets the mating surface, the extended area of the ball hard pressed the cladding surface. As a result, adhesion and scuff occurred [36], which stuck the movement between the ball and plate. But, the wear loss and frictional force were minimal. The material pile-up and depth of wear was less on the laser-cladded wear track. The formation of dendrite structure with higher hardness may be the reason for less material loss [4]. The improved properties are supposed to be the joint solution of the uniform distribution of hard phase, grain-refining effect and good bonding between powders and matrix.

In the present wear study, abrasives and adhesives are the most important wear mechanisms. The adhesive wear was happening while the coated surface touches directly the mating surface. Whereas, abrasive wear is an effect of roughness at the counterpart surface and/or debris that stay on the wear path may work as abrasive mediators. After sliding some distance, the harder ball creates a track on the cladded surface to remove the material as debris [37]. Further, while the cladded surface slides on the ball, it tends to pull and press the debris on the wear track. Both abrasive and adhesive mechanisms were happening more or less simultaneously. The cladded surface sliding on the counterpart is exposed to adhesive wear whereas, at the front of it, a pile-up of debris is being pushed causing abrasive wear.

A schematic illustration of the series of stages happening while hardened tungsten carbide ball slides on the cladded surface is shown in Fig. 12. As the hardened counterpart contacts and sliding over the cladded surfaces, the harder NiCrSiBC which cladded in the titanium alloy surface raises the contact pressure at the interface. As an outcome, the matrix can be deformed and adheres to the counterpart [43]. The removed material can be joined together and performed as a wedge to support further material removal. The hardened ball continues the sliding on the cladded surface and removes the adhesive wear results of the matrix material. Therefore, this scratched uneven surface causes an abrasive wear.

**Fig. 12** Schematic illustration of the adhesive wear at the interface matrix/boride **a** before sliding, **b** the hardened ball sliding over the cladded plate with high contact pressure and **c** after sliding with piled-up material (adhesive)



Furthermore, on laser cladding surface, the main mechanism is grooving in both matrix and strengthening phases. Hence, the observed differences in the wear mechanism with coating microstructure can be associated to the creation of large floret-shape chromium borides in NiCrSiBC coating. Normally, these types of large-size nickel, silicon and chromium borides perform as load-bearing areas. da Silva et al. [44] investigated the enhancement of wear resistance on formation of floret-shape  $\text{Cr}_5\text{B}_3$  and is illustrated in Fig. 13. On the floret shape  $\text{Cr}_5\text{B}_3$ , the abrasive particles experience a lesser distance ( $\Delta D_1$ ) between both surfaces with relatively higher load ( $\Delta F_1$ ). At this moment, the nickel-based matrix is higher worn compared with hard borides ( $\text{Cr}_5\text{B}_3$ ). Now, the abrasive particles were moved into translational motion and forming grooves on the  $\text{Cr}_5\text{B}_3$  boride surface. But, when the abrasive particles move along with the matrix (Ni), the gap between two surfaces will increase ( $\Delta D_2 > \Delta D_1$ ) and the applied load becomes lesser ( $\Delta F_2$ ). In this stage, the surface (Ni clad) gets a higher significant wear when compared with chromium boride ( $\text{Cr}_5\text{B}_3$ ), allowing rotational movements which can cause microrolling on the nickel-based clad surface [45].

Normal applied force ( $\Delta F_1$ )

> Normal applied force ( $\Delta F_2$ )

Initial distance between surface ( $\Delta D_1$ )

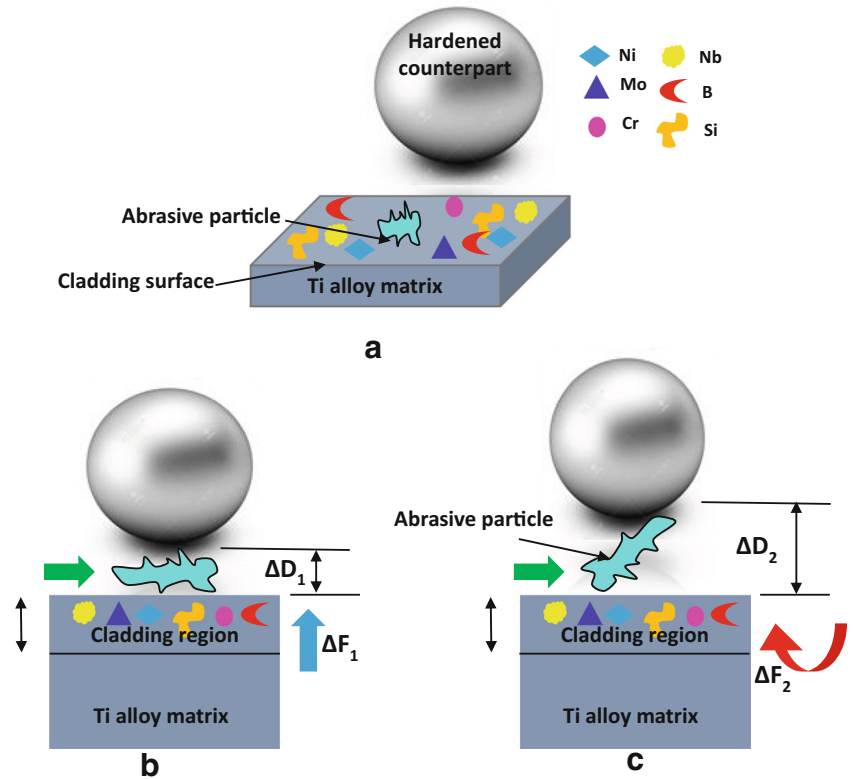
> Final distance between surface ( $\Delta D_2$ )

where  $F$  is the applied force and  $D$  the distance between surfaces.

### 3.6 Whitelight interferometer analysis

Figure 14 shows the worn-out cladded and unclad surface roughness. The unclad worn-out surface shows higher surface roughness of  $\sim 6.3 \mu\text{m}$ . This was due to lower hardness and higher material loss of the titanium alloy. The NiCrMoNb- and NiCrSiBC-cladded surface shows the lower roughness  $\sim 3.2$  and  $\sim 2.3 \mu\text{m}$ , respectively, after wear test. The  $\gamma$ -Ni

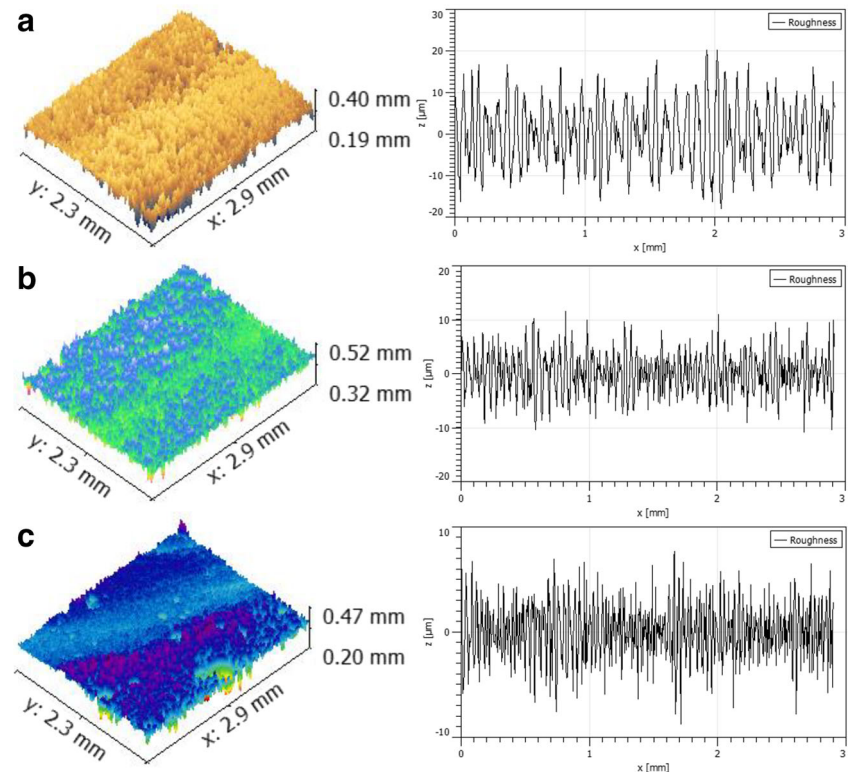
**Fig. 13** Schematic picture of the interaction between abrasive particle and NiCrSiBC/NiCrMoNb phases **a** before sliding, **b** the counterpart sliding over the abrasive particle with  $D_1$  distance and **c** the counterpart sliding over the abrasive particle with  $D_2$  distance



was mixed with chromium, borides and silicon and formed the structure of interdendritic eutectics, which can provide a strong network to enhance the wear resistance of cladding

layer. Comparing with NiCrMoNb and unclad specimen, the NiCrSiBC-cladded worn-out surfaces exhibited a reduction in roughness averages.

**Fig. 14** Worn out pin surfaces of **a** substrate, **b** NiCrMoNb and **c** NiCrSiBC cladding samples



## 4 Conclusions

This present study was done to examine and compare the phase analysis, hardness, microstructure and wear resistance of both NiCrMoNb and NiCrSiBC laser claddings. Based on the experimental results, the following conclusions were drawn.

- Both claddings such as NiCrMoNb and NiCrSiBC were free from defects such as crack and porosity and achieved good metallurgical bonding with substrate material. The coating microstructure shows a finer and dendrite structure due to higher cooling rate. The element distribution and hardness proved that the coating has a homogeneous structure.
- Moreover, the hardness measurement of NiCrSiBC cladding shows a higher cladding than that of NiCrMoNb. In NiCrSiBC coating, the elements such as carbon, boron and chromium were segregated as carboborides and carbides.
- The material loss on the substrate is more than NiCrMoNb and NiCrSiBC cladding surfaces. This happened due to the enhancement of base metal hardness after laser cladding with NiCrMoNb and NiCrSiBC powders. In the cladding period,  $\gamma$ -Ni was mixed with chromium, borides, silicon and molybdenum and formed the structure of interdendritic eutectics, which can provide a strong network to enhance the wear resistance of cladding layer.
- In wearing-in stage of both clad NiCrMoNb and NiCrSiBC coatings show instable friction coefficient, and after sliding some distance, the coefficient of friction was constant. This behaviour may be attributed to various wear mechanisms during wear test.
- Abrasive and adhesive are major wear mechanisms found in this study. Comparing with NiCrMoNb and unclad specimen, the NiCrSiBC-clad worn-out surfaces exhibited reduction in roughness averages. Finally, the NiCrSiBC cladding can be considered an alternative to the NiCrMoNb coating.

**Funding information** The authors wish to thank the Ministry of Science and Technology (MOST), Taiwan (Republic of China) for providing financial support to carry out this research work.

## References

- Zhu YY, Liu D, Tian XJ, Tang HB, Wang HM (2014) Characterization of microstructure and mechanical properties of laser melting deposited Ti-6.5Al-3.5Mo-1.5Zr-0.3Si titanium alloy. *Mater Des* 56:445–453
- Mthisi A, Popoola API, Popoola OM (2019) Tribological behaviour of laser synthesized Ti-Al<sub>2</sub>O<sub>3</sub> coatings on Ti-6Al-4V alloy. *Int J Adv Manuf Technol* 103:655–664
- Fu YQ, Batchelor AW (1998) Laser nitriding of pure titanium with Ni, Cr for improved wear performance. *Wear* 214:83–90
- Jeyaprakash N, Duraiselvam M, Raju R (2018) Modelling of Cr<sub>3</sub>C<sub>2</sub>-25% NiCr laser alloyed cast iron in high temperature sliding wear condition using response surface methodology. *Arch Metall Mater* 63:1303–1315
- Gu DD, Hagedorn YC, Meiners W, Meng GB, Batista RJS, Wissenbach K et al (2012) Densification behavior, microstructure evolution, and wear performance of selective laser melting processed commercially pure titanium. *Acta Mater* 60:3849–3860
- Jeyaprakash N, Yang C-H, Muthukannan D, Prabu G, Sheng-Po T, Raj Kumar D (2019) Investigation of high temperature wear performance on laser processed nodular iron using optimization technique. *Results Phys* 15:102585
- Jeyaprakash N, Yang C-H, Tseng S-P (2019) Wear Triboperformances of laser cladding Colmonoy-6 and Stellite-6 micron layers on stainless steel 304 using Yb:YAG disk laser. *Met Mater Int*:1–14. <https://doi.org/10.1007/s12540-019-00526-6>
- Xi W, Song B, Yu Z, Yu T, Wang J (2019) Geometry and dilution rate analysis and prediction of laser cladding. *Int J Adv Manuf Technol* 103:4695–4702
- Xu X, Mi G, Xiong L, Jiang P, Shao X, Wang C (2018) Morphologies, microstructures and properties of TiC particle reinforced Inconel 625 coatings obtained by laser cladding with wire. *J Alloys Compd* 740:16–27
- Zhuang Q, Zhang P, Li M, Yan H, Yu Z, Lu Q (2017) Microstructure, Wear resistance and oxidation behavior of Ni-Ti-Si coatings fabricated on Ti6Al4V by laser cladding. *Materials* 10:1248
- Yin M, WenjianWang WH, Cai Z (2018) Impact-sliding tribology behavior of TC17 alloy treated by laser shock peening. *Materials* 11:1229
- Hemmati I, Ocelik V, DeHosson JTM (2012) Dilution effects in laser cladding of Ni-Cr-B-Si-C hardfacing alloys. *Mater Lett* 84:69–72
- Ramasubbu V, Chakraborty G, Albert SK, Bhaduri AK (2011) Effect of dilution on GTAW Colmonoy 6 (AWS NiCr-C) hardface deposit made on 316LN stainless steel. *Mater Sci Technol* 27(2):573–580
- Fernandes F, Cavaleiro A, Loureiro A (2012) Oxidation behavior of Ni-based coatings deposited by PTA on gray cast iron. *Surf Coat Technol* 207:196–203
- Hemant K, Ramakrishnan V, Albert SK, Bhaduri AK, Ray KK (2017) Friction and wear behaviour of Ni-Cr-B hardface coating on 316LN stainless steel in liquid sodium at elevated temperature. *J Nucl Mater* 495:431–437
- Sassatelli P, Bolelli G, Gualtieri ML, Heinonen E, Honkanen M, Lusvardi L, Manfredini T, Rigon R, Vippola M (2018) Properties of HVOF-sprayed Stellite-6 coatings. *Surf Coat Technol* 338:45–62
- Ferozhkhan MM, Duraiselvam M, Kumar KG, Ravibharath R (2016) Plasma transferred arc welding of Stellite 6 alloy on stainless steel for wear resistance. *Procedia Technol* 25:1305–1311
- Sidhu TS, Prakash S, Agrawal RD (2006) Hot corrosion resistance of high-velocity oxyfuel sprayed coatings on a nickel-base superalloy in molten salt environment. *J. Therm. Spray Technol.* 15:387–399
- de Oliveira U, Ocelik V, De Hosson JTM (2007) Microstresses and microstructure in thick cobalt-based laser deposited coatings. *Surf Coat Technol* 201:6363–6371
- Kusmoko A, Dunne D, Li H, Nolan D (2014) Effect of two different energy inputs for laser cladding of Stellite 6 on P91 and P22 steel substrates. *Procedia Mater Sci.* 6:26–36
- Bartkowski D, Młynarczyk A, Piasecki A, Dudziak B, Gościński M, Bartkowska A (2015) Microstructure, microhardness and corrosion resistance of Stellite-6 coatings reinforced with WC particles using laser cladding. *Opt Laser Technol* 68:191–201



22. Calleja A, Urbikain G, González H, Cerrillo I, Polvorosa R, Lamikiz A (2018) Inconel®718 superalloy machinability evaluation after laser cladding additive manufacturing process. *Int J Adv Manuf Technol* 97:2873–2885
23. ASTM International (2010) ASTM Standard G: 99-05. Standard test method for wear testing with a pin-on-disk apparatus. ASTM International, PA
24. Atanu C, Raghupathy Y, Srinivasan D, Suwas S, Srivastava C (2017) Microstructural evolution of cold-sprayed Inconel 625 superalloy coatings on low alloy steel substrate. *Acta Mater* 129:11–25
25. Xu X, Mi G, Chen L, Xiong L, Jiang P, Shoa X, Wang C (2017) Research on microstructures and properties of Inconel 625 coatings obtained by laser cladding with wire. *J Alloys Compd* 715:362–373
26. Huebner J, Rutkowski P, Kata D, Kusinski J (2017) Microstructural and mechanical study of Inconel 625—tungsten carbide composite coatings obtained by powder laser cladding. *Arch Metall Mater* 62(2):531–538
27. Zhang H, Shia Y, Kutsuna M, Xu GJ (2010) Laser cladding of Colmonoy 6 powder on AISI316L austenitic stainless steel. *Nucl Eng Des* 240:2691–2696
28. Conde A, Zubiri F, de Damborenea J (2002) Cladding of Ni–Cr–B–Si coatings with a high power diode laser. *Mater Sci Eng A* 334: 233–238
29. Zheng ML, Sun HQ, Liu WJ (2005) *Scr. Mater.* 53(2):159–753
30. Kou S (2017) *Welding metallurgy*. John Wiley and Sons
31. Abioye TE, Folkes J, Clare AT (2015) *J Mater Process Technol* 217: 232–240
32. Abioye TE, Folkes J, Clare AT (2013) A parametric study of Inconel 625 wire laser deposition, *J Mater Process Technol* 213(12):2145–2151
33. Abioye TE (2014) Laser deposition of Inconel 625/tungsten carbide composite coatings by powder and wire feedstock. PhD thesis, University of Nottingham
34. Corchia M, Delogu P, Nenci F (1987) Microstructural aspects of wear-resistant Stellite and Colmonoy coatings by laser processing. *Wear* 119:137–152
35. Paul CP, Jain A, Ganesh P, Negi J, Nath AK (2006) Laser rapid manufacturing of Colmonoy-6 components. *Opt Lasers Eng* 44: 1096–1109
36. Jeyaprakash N, Yang C-H, Muthukannan D, Prabu G (2019) Microstructure and tribological evolution during laser alloying WC-12%Co and Cr<sub>3</sub>C<sub>2</sub>-25%NiCr powders on nodular iron surface. *Results Phys* 12:1610–1620
37. Jeyaprakash N, Muthukannan D, Aditya SV (2018) Numerical modeling of WC-12% Co laser alloyed cast iron in high temperature sliding wear condition using response surface methodology. *Surf Rev Lett* 25(7):1950009
38. Li P, Wu LY, Guiong YM, Liu X (2012) Distribution of TiB<sub>2</sub> particles and its effect on the mechanical properties of A390 alloy. *Mater Sci Eng A* 546:146–152
39. Kesavan D, Kamaraj M (2010) The microstructure and high temperature wear performance of a nickel base hard faced coating. *Surf Coat Technol* 204:4034–4043
40. Gholipour A, Shamanian M, Ashrafizadeh F (2011) Microstructure and wear behavior of Stellite 6 cladding on 17-4 PH stainless steel. *J Alloys Compd* 509:4905–4909
41. Feng K, Chen Y, Deng P, Li Y, Zhao H, Lu F, Li R, Huang J, Li Z (2017) Improved high-temperature hardness and wear resistance of Inconel625 coatings fabricated by laser cladding. *J Mater Process Technol* 243:82–91
42. Waterhouse RB, Wharton MH (1974) Titanium and tribology. *Ind Lubr Tribol* 26(1/2):20–23
43. da Silva LJ, C.M. D'Oliveira AS (2016) NiCrSiBC coatings: effect of dilution on microstructure and high temperature tribological behaviour. *Wear* 350–351:130–140
44. da Silva LJ, Scheuer CJ, C.M. D'Oliveira AS (2019) Effect of microstructure on wear performance of NiCrSiBC coatings. *Wear* 428–429:387–394
45. Cozza RC (2014) Third abrasive wear mode: is it possible? *J Mater Res Technol* 3:191–193

**Publisher's note** Springer Nature remains neutral with regard to jurisdictional claims in published maps and institutional affiliations.